Tectonophysics 588 (2013) 27–38

Contents lists available at SciVerse ScienceDirect

Tectonophysics

journal homepage: www.elsevier.com/locate/tecto

# Eocene seawater retreat from the southwest Tarim Basin and implications for early Cenozoic tectonic evolution in the Pamir Plateau

Jimin Sun *, Maosheng Jiang

*Key Laboratory of Cenozoic Geology and Environment, Institute of Geology and Geophysics, Chinese Academy of Sciences, P. O. Box 9825, Beijing 100029, China*

ARTICLE INFO

*Article history:*
Received 13 June 2012
Received in revised form 23 November 2012
Accepted 26 November 2012
Available online 8 December 2012

*Keywords:*
Neotethys Ocean
Cenozoic
Pamir Plateau
Tarim Basin

ABSTRACT

The Pamir Plateau lies in the western end of the India–Eurasia collision zone, being an unusual example for studying crustal shortening and evolution of the Neotethys Ocean. Here we present new results from the southwestern margin of the Tarim Basin for discussing tectonic history in the northern Pamir Plateau as well as for providing precise dates of the final seawater retreat from the studied region. Our results indicate that early uplift of the northern edge of the Pamir Plateau occurred at about 55 Ma, but this uplift preceded the closure of the link between the Neotethys and the Tarim Basin. Five marine transgression and regression cycles occurred during the early Eocene, mostly in response to global eustatic sea level fluctuations, and the final seawater retreat from the southwest Tarim Basin occurred at about 47 Ma. Another uplift episode started 34 Ma, supported by the accumulation of coarse molasse deposits as well as our palynological evidence, suggesting that the convergence between the Pamir Plateau and the Tian Shan ranges accelerated since the beginning of the early Oligocene.



## 1. Introduction

The Pamir Plateau is one of the most prominent ongoing crustal deformation regions on earth, located at the western end of the India–Eurasia collision zone (Fig. 1a and b). This region is marked by the junction of a series of world highest mountains including the Himalayas, Tian Shan, Karakoram, Kunlun, and Hindu Kush ranges. Formation of the Pamir Plateau was associated with the northward displacement of the India Plate, and this area has experienced remarkable crustal shortening during the Cenozoic era (Abers et al., 1988; Bershaw et al., 2012; Burtman, 2000; Burtman and Molnar, 1993; Burtman et al., 1996; Fu et al., 2010; Molnar and Tapponnier, 1975; Negredo et al., 2007; Robinson et al., 2004, 2007; Tapponnier et al., 2001; Yin and Harrison, 2000). In the present, the Pamir Plateau is known as the "Roof of the World", belonging to the Western Himalayan Syntaxis. Given the specific location, the Pamir Plateau is an ideal region for study of crustal shortening, mountain building, and the evolution of the Neotethys Ocean in the western syntaxis of the India–Asia collision zone. However, such questions have been hampered by poor stratigraphic knowledge and uncertain chronology of the Cenozoic deposits in the foreland basins of the Pamir Plateau.

In this paper we focused on studying marine and terrestrial Tertiary sedimentary rocks accumulated in an evolving northeastern margin of the Pamir Plateau (Fig. 1b), where large volumes of sediments eroded from the rising mountains of the West Kunlun and Pamir Plateau accumulated in the southwestern Tarim Basin forming deformed Cenozoic strata of up to 10 km thick.

The aims of this paper are to: (i) construct a high resolution magnetostratigraphy of Paleogene deposits in the southwest Tarim Basin; provide precise chronology of seawater retreat from the region studied; and (ii) explore crustal shortening history between the Pamir Plateau and the Tian Shan.

## 2. Geological setting and stratigraphy

The study area is the southwest Tarim Basin, constrained by the Pamir Plateau to the west and the west Kunlun range to the south (Fig. 1b). Today, most of the basin itself is covered by a large sand sea called Taklimakan, and arid climate has prevailed at least since the latest Miocene (Sun and Liu, 2006; Sun et al., 2008, 2009; Zheng et al., 2010). Field investigations indicate that the present dune sands occupy most of the basin interior, whereas the marginal Tarim Basin is characterized by thrusting and folding zones consisting of Mesozoic to Cenozoic strata (Pan, 2000; Sobel and Dumitru, 1997). The studied Oytag section is located in the southwest Tarim Basin, exposed by the northward flowing Gez River (Fig. 2), which originates from the Pamir Plateau. This section consists of Paleocene to Oligocene deposits, and field observation indicates that all these Paleogene strata are tectonically overturned (Fig. 3).

The 3680 m-thick deposits can be divided into three units. The Paleocene strata are terrestrial red beds consisting of laminated sandstone and siltstone in the lower part (Fig. 4a) and alternatively accumulated reddish siltstone and coarse gray gravels in the upper part. The sedimentary facies of the Paleocene strata suggest fluvial–lacustrine

* Corresponding author. Tel.: +86 10 8299 8389.
*E-mail address:* jmsun@mail.igcas.ac.cn (J. Sun).

0040-1951/$ – see front matter © 2012 Elsevier B.V. All rights reserved.
http://dx.doi.org/10.1016/j.tecto.2012.11.031

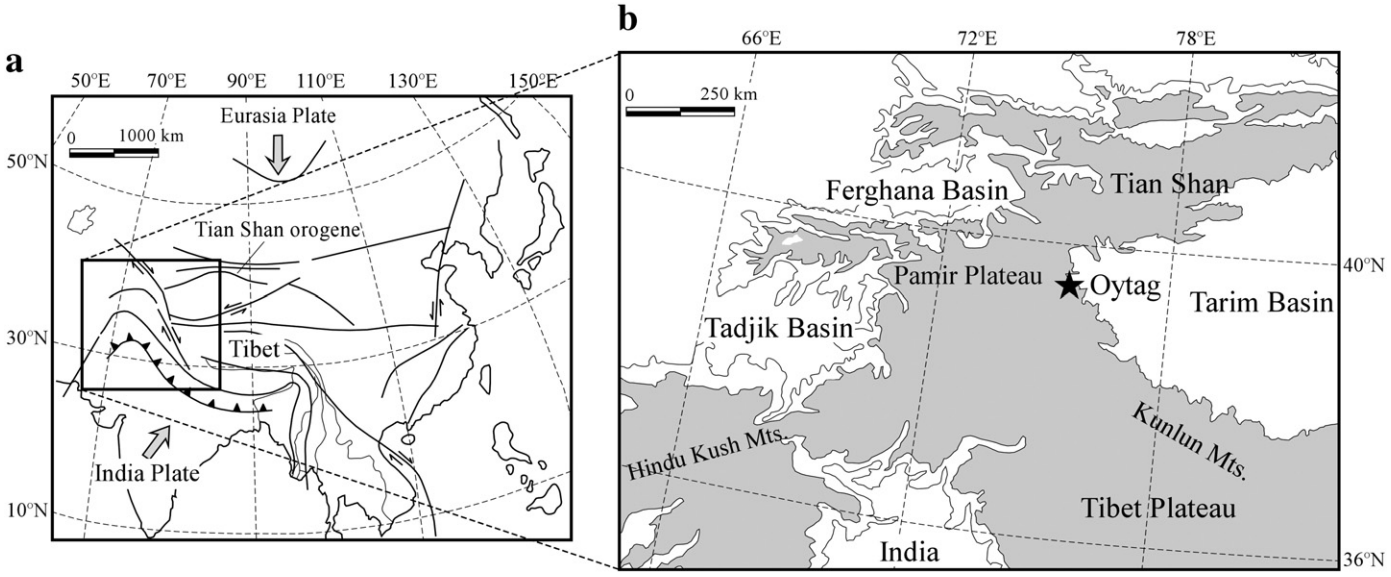


**Fig. 1.** Maps showing the tectonic and topographic frameworks of the Pamir Plateau. (a) Schematic tectonics in central Asia. (b) The topography of the study region and the location of the Oytag section; the shadow indicates mountain elevations > 2000 m.

deposition environment in the early time and high energy fluvial to fan deposits in the late stage. There is a sharp contact between the Paleocene and Eocene deposits characterized by a change from terrestrial deposits to the early Eocene marine gypsum evaporates.

The lower part of the Eocene deposits is dominated by interbedding marine–terrestrial lithofacies, characterized by five intercalated marine limestone beds (named as I, II, III, IV, and V upwards, Fig. 3). A right-lateral striking fault can be identified within the earliest Eocene marine strata (Figs. 3 and 5). Field observations indicated that the offset distance of the fault is only about 50 m (Fig. 5). Marine ostracoda fossils (e.g., cf. *Propontocypris wuqiaensis* Gou, cf. *Laxoconcha invonuta* Mandelstam, and *Cytherella* cf. *antermarginata* Babinot were identified from the lowest limestone bed, and *Cytherella retrorsa* Mandelstam, *Haplocytheridea* sp., and *Pontocypris* cf. *elongatissima* Mandelstam) were found in the two lower limestones, while bivalve fossils (e.g., *Venericardia* cf. *hortensis* (Vinassa de Regny), *Flemingostrea kaschgarica* Vyalov, *Cardita* cf. *suessi* Koenen) or fragments were found from the other three limestones (Fig. 3). The rock types of the limestones are dominated by marl, wackstone, packstone and bioclastic packstone, and the sedimentary facies include carbonate platform and shallow, evaporative tidal flat (Tang et al., 1992).

The middle part of the Eocene deposits is terrestrial reddish laminated to massive mudstone (Fig. 4c), showing horizontal bedding and suggesting low-energy lacustrine environment.

The upper part of the terrestrial Eocene deposits is dominated by laminated to massive mudstone but occasionally with interbedded layers of gray gravels, suggesting a dominant lake environment. There are two small tight folds within this part (Fig. 3).

The Oligocene strata are typical terrestrial molasse deposits marked by alternations of brownish laminated sandstone/siltstone and coarse gray conglomerates (Fig. 4d). Field investigations indicate that the uppermost part of the Oligocene strata was eroded, and a tight fold occurred in the lower part (Fig. 3), moreover, there is a sedimentary hiatus between the Oligocene molasse deposits and the underlying Eocene mudstone (Fig. 3). The sedimentary facies can be interpreted as high-energy flood or fan systems.

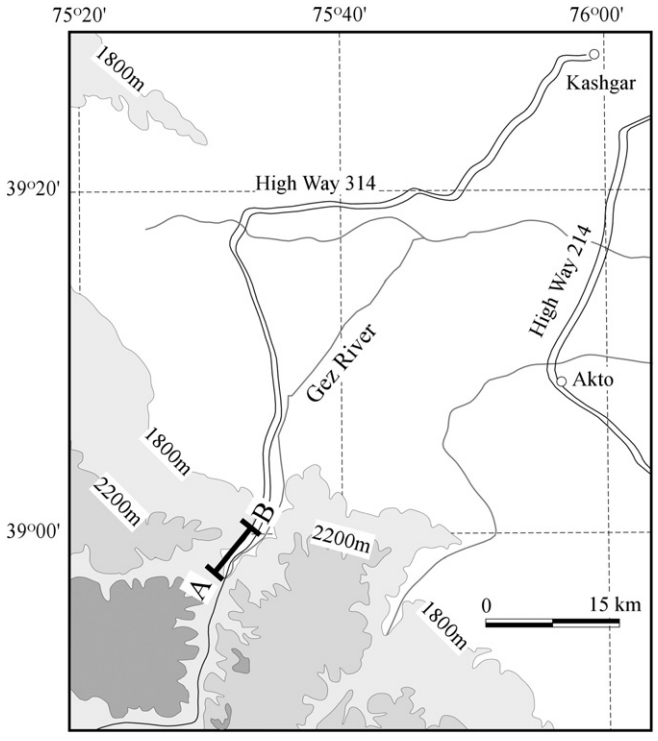


**Fig. 2.** Map showing the detailed geographic location of the study region and the sampling route (along transection A–B).

## 3. Materials and methods

During our field expeditions in the years 2006, 2007, and 2012, up to 1002 oriented specimens from 501 sampling sites were taken, wherein at every sampling position, we drilled two samples. All the samples were cored with a portable gasoline-powered drill and oriented in the field measuring immersion and inclination by using an inclinometer for deterring inclination (dip) of the core axis and magnetic compass (Suunto MC-2) for determining azimuth. The accuracy of orientation by such methods is about ±2°.

All samples were subjected to stepwise thermal demagnetization by using a magnetic measurement thermal demagnetizer (MMTD Model 80). In general, thermal demagnetization intervals are 25–50 °C below 610 °C and 10–20 °C above 610 °C. Magnetic remanence was measured with a 2G-760 U-channel, three-axis, cryogenic magnetometer housed in field-free space (<300 nT), at the Paleomagnetism and Geochronology Laboratory of the Institute of Geology and Geophysics, Chinese Academy

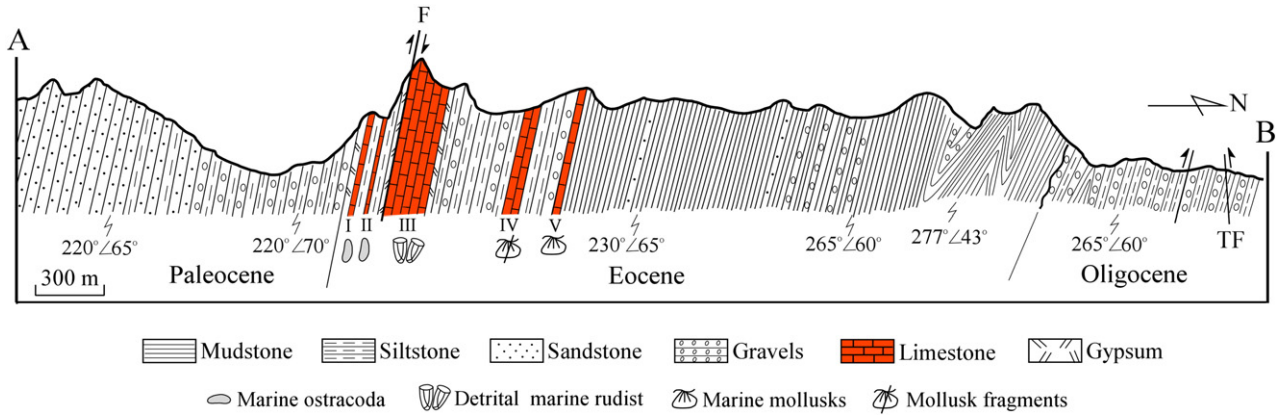


**Fig. 3.** Cross-section of the Oytag section showing the Paleocene to Oligocene strata. TF: thrust fault.

of Sciences. The characteristic directions of magnetization were determined by least squares fitting (Kirschvink, 1980) through selected demagnetization data points (minimum of three, but typically four to eight), and directions were analyzed using Fisher statistics (Fisher, 1953).

Mineral magnetic measurements were also performed for selected samples. The temperature dependent magnetic susceptibilities were measured using a KLY-3 Kappabridge with a CS-3 high-temperature furnace in an argon atmosphere. The sample holder and thermocouple contributions to magnetic susceptibility were subtracted.

Because the U–Pb ages of detrital zircons obtained from clastic sedimentary rocks provide important constraints for evaluating the ages of the potential source materials. In this study, we separated zircons from two sandstone samples collected at two stratigraphic positions at Oytag section. Cathodoluminescence (CL) images were obtained for the zircons prior to analysis, using a CAMECA SX-50 microprobe at the Institute of Geology and Geophysics, Chinese Academy of Sciences (IGGCAS) in Beijing, in order to characterize internal textures and choose potential target sites for U–Pb dating. U–Pb dating for zircon was determined by using a Neptune MC-ICP-MS and Agilent Q-ICP-MS, equipped with a 193 nm excimer laser ablation system at the IGGCAS. The detailed analytical technique is described in Xie et al. (2008).

We also performed pollen study on selected bulk samples. For pollen analysis, at least 100 g of sediment was used. Samples were treated with HCl (35%) and HF (70%) to remove carbonates and silica. Separation of the palynomorphs from the residue was performed by using $ZnCl_2$ (density = 2), following the method of Faegri and Iversen (1989). Slides were prepared by mounting the pollen grains in glycerin jelly, and then counted under a microscope using ×400 magnifications.

Eighteen samples were collected for Ca and Sr analyses from the limestone Beds III, IV, and V. Measurements were carried out at the Institute of Geology and Geophysics, Chinese Academy of Sciences, determined by using an inductively coupled plasma optical emission spectrometer (ICP-OES). Analytical uncertainties were less than 3%.

## 4. Results

### 4.1. Rock magnetic experimental results

Analysis of the temperature dependence of the magnetic susceptibility of the heating curves shows noticeable decreases of the magnetic susceptibility around temperatures of 580 °C and 680 °C (Fig. 6), indicating the existence of magnetite and hematite, respectively. Because the bulk susceptibility of magnetite is ~1000 times greater than most

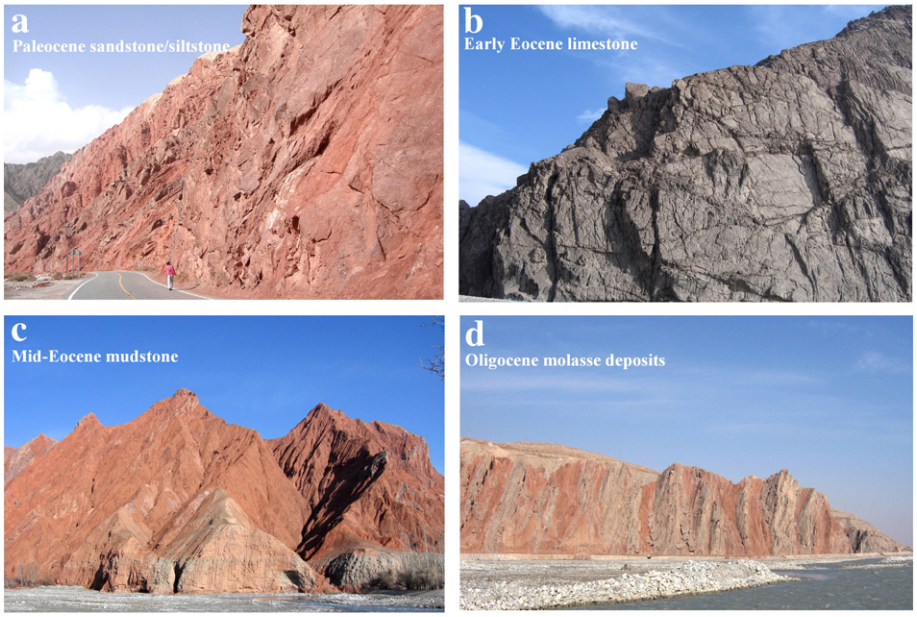


**Fig. 4.** Photos show the Paleogene deposits at Oytag. (a) The Paleocene terrestrial reddish sandstone/siltstone. (b) Early Eocene dark gray marine limestone. (c) Dominant reddish mid-Eocene mudstone. (d) Gray conglomerates with interbedded brownish siltstone/sandstone of Oligocene age.


**Fig. 5.** Photo shows the right-lateral strike-slip fault disrupting the early Eocene marine strata with an offset distance of about 50 m.

rock materials (Collinson, 1983), this thermomagnetic behavior suggests that the magnetic minerals are dominated by hematite, with magnetite present as a subordinate ferromagnet.

### 4.2. Demagnetization

The intensity of the natural remanent magnetization (NRM) of most specimens was of the order of $10^{-3}$ A/m. Among the 501 oriented specimens, 431 samples successfully isolated the characteristic remanent magnetization (ChRM) after removal of one or two soft secondary components of magnetization. 70 specimens could not be isolated by stable ChRM but show erratic demagnetization behavior. Representative demagnetization diagrams are shown in Fig. 7. For most samples, three magnetic components were isolated (Fig. 7a–f and h–i): the low (below 250 °C) component does not decay toward the origin, the middle (250–585 °C) points constitute an intermediate component, while a high temperature (585–670 °C) component carries the characteristic remanent magnetization (ChRM) direction. Another thermal demagnetization behavior (Fig. 7g) is characterized by the two component magnetization: a low temperature magnetic component was removed by thermal demagnetization at about 400–450 °C, and another component above 450 °C carries the ChRM direction.

### 4.3. U–Pb detrital zircon analytical results

The sizes of the separated zircons range from 70 to 200 μm. The cathodoluminescence images show that most zircons are euhedral to slightly rounded, and most of the zircons exhibit oscillatory cathodoluminescence zoning characteristic (Fig. 8), being generally considered to be of magmatic origin (e.g., Hanchar and Miller, 1993). We analyzed 160 zircon grains: 83 grains from sample YT001, and 77 grains from YT002.

Zircon U–Pb isotopic results of the two samples are presented in concordant diagrams (Fig. 9). For the sample YT001, four major groups can be identified: at 2600 to 2400, 1900 to 1700, 1200 to 900, and 500 to 245 Ma (Fig. 9a). The two youngest grains have $^{206}Pb/^{238}U$ ages ranging from 52 to 44.9 Ma with a weighted mean age of $44.9 \pm 0.8$ Ma. For the sample YT002, generally four groups of ages can be identified; they are 2600–2200, 2000–1800, 1000–700, and 450–250 Ma (Fig. 9b). Two grains yield the youngest $^{206}Pb/^{238}U$ age of 42.75 Ma.

For the detrital zircon samples, the youngest U–Pb ages provide the maximum ages of the sedimentary succession. Therefore, the youngest ages of the two samples give the upper limits for the corresponding strata.

### 4.4. Chronology of the Oytag section

The time scale of the studied section is based on multiple chronologies of biostratigraphic age control, detrital zircon ages, and paleomagnetic polarity. In this study, ostracoda fossils of cf. *P. wuqiaensis* Gou, cf. *L. invonuta* Mandelstam, and *C.* cf. *antermarginata* Babinot were identified from the lowest limestone bed (Bed I, Fig. 3), and *C. retrorsa* Mandelstam, *Haplocytheridea* sp., and *P.* cf. *elongatissima* Mandelstam were identified from the second limestone (Bed II, Fig. 3). Some of the ostracoda fossils suggest Paleocene to Eocene age, and all of them are stenohaline marine species. Three fossil zones of bivalve fossils or fragments were discovered from the other limestone beds (Fig. 3). Firstly, benthic marine fossil of *Biradiolites boldjuanensis* Bobkova was collected from the thickest limestone of Bed III (Fig. 3). Such fossil is generally regarded as late Cretaceous age (Lan and Wei, 1995; Scott et al., 2010). However, our field observations indicate that these fossils were preserved in a large boulder, and the well-rounded shape of the boulder (Fig. 10) implies that it was not in situ but re-transported. Therefore, the late Cretaceous age of the fossils does not represent the age of the strata. This can be further supported by our pollen analysis of the section which indicates that all the pollen taxa are Cenozoic pollen elements. The lithology of the limestone Bed III is dominated by marl and wackstone, representing a shallow-marine carbonate platform environment (Tang et al., 1992).

For the limestone Bed IV, although we did not find well-preserved bivalve fossils, plenty of fragments of bivalve fossils can be easily identified, being bioclastic packstone. On the basis of regional stratigraphic correlation, the sedimentary face of this limestone was regarded as representing a marine subtidal zone (Tang et al., 1992).

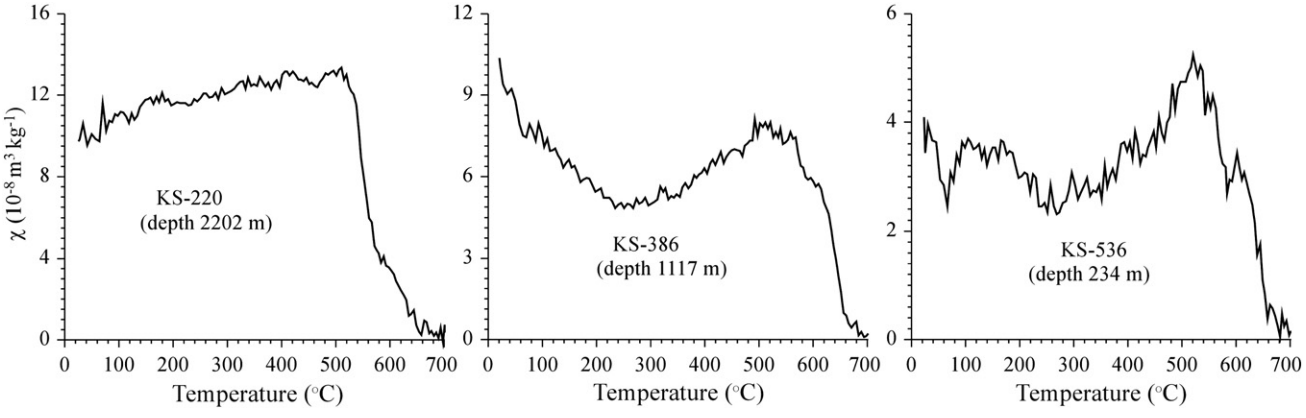


**Fig. 6.** Temperature dependence of magnetic susceptibility (*k*–T curves) for representative samples from different levels of the section. All spectra were determined by heating from room temperature to 700 °C in argon gas atmosphere.

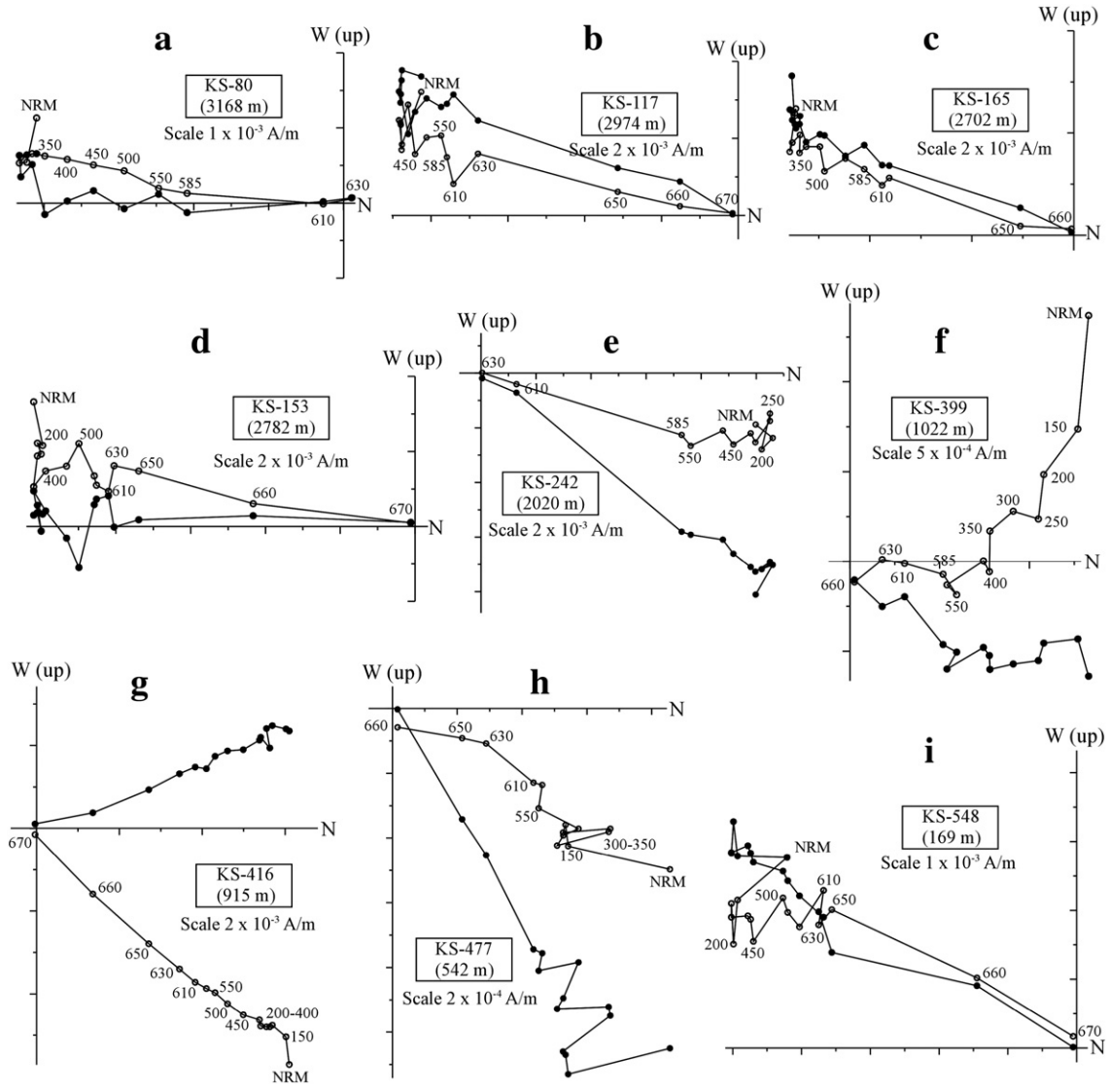


**Fig. 7.** Orthogonal demagnetization diagrams showing typical thermal demagnetization behaviors of the studied samples. Demagnetization steps are in °C in all plots, and directions are plotted in situ. NRM is the natural remanent magnetization. Solid and open circles represent vector endpoints projected onto the horizontal and vertical planes, respectively.

The fossil zone of marine bivalve fossils was collected from the uppermost marine limestone Bed V (Fig. 3), including *V. hortensis*, *F. kaschgarica* Vialov, and *C. suessi* Koenen, such in situ fossils were attributed to an age of early Eocene in the Tarim Basin representing shallow sea environment (Lan and Wei, 1995). Moreover, *V. hortensis* is identical to the specimens from the early Eocene of France and Turkey (Okan and Hosgor, 2009), suggesting that similar environmental conditions existed between the different parts of the Neotethys seas either in the Tarim Basin or in Europe. Such biostratigraphic age control is essential for correlating and examining our magnetostratigraphic time scale.

Except the biostratigraphic age control, the U–Pb ages of detrital zircons from sandstones can also provide age constrains on the deposits of the Oytag section. The two samples taken from the middle

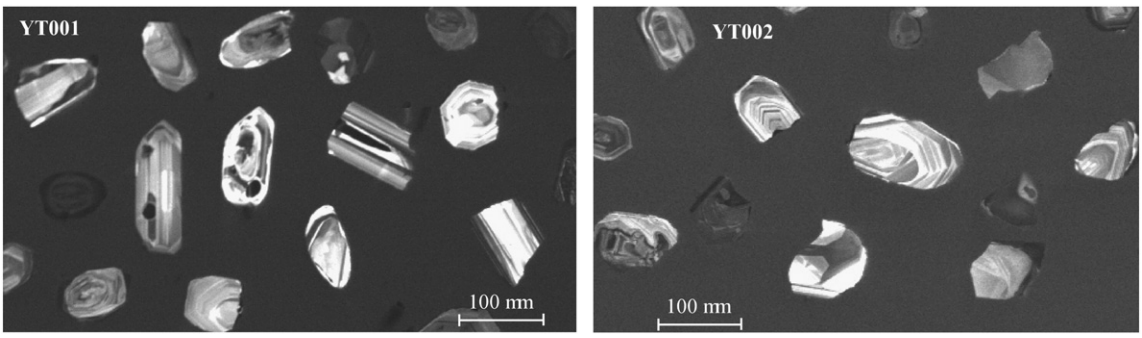


**Fig. 8.** Representative cathodoluminescence images for detrital zircons from the Oytag section. The shapes of the zircons change from sun-rounded to euhedral.

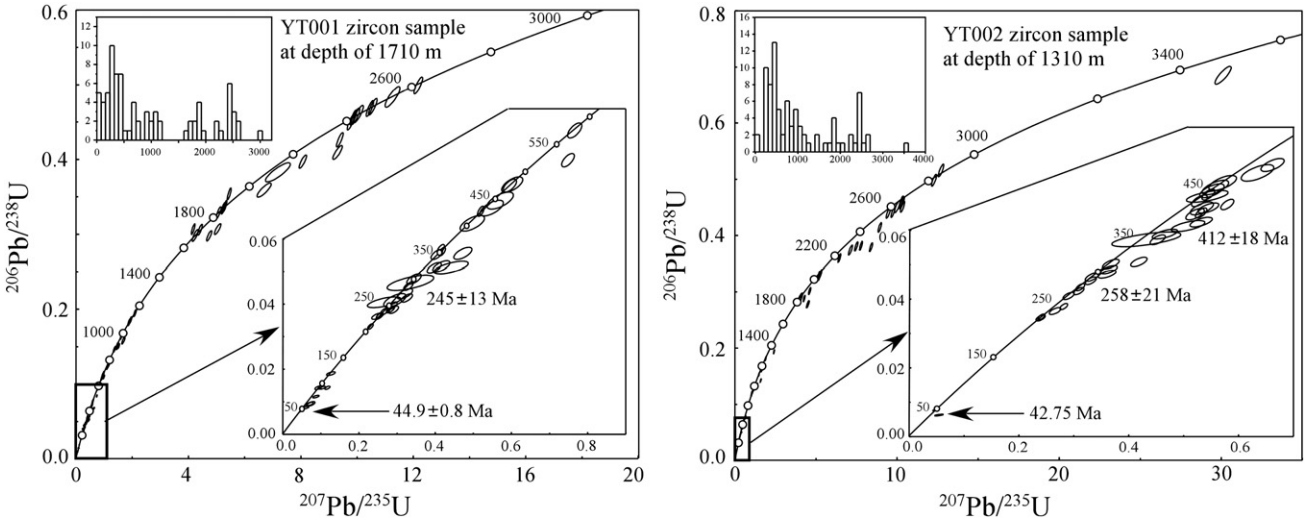


**Fig. 9.** U–Pb concordia diagrams for detrital zircons from the Oytag section. The inset is a histogram of the distribution of $^{207}Pb/^{206}Pb$ ages.

part of the sections at depths of 1710 and 1310 m yielded the youngest zircon ages of 44.9 ± 0.8 Ma and 42.75 Ma, respectively (Fig. 11). These ages indicate a maximum depositional age of late Eocene for the middle part of the section, which was accumulated after seawater retreat from the studied region.

Based on the above biostratigraphic chronology and detrital zircon ages, we can correlate our magnetostratigraphy to the standard polarity time scale to generate high resolution age control for the Oytag section. The declination and inclination obtained for the characteristic remanent magnetization of the specimens were used to calculate the virtual geomagnetic pole (VGP) latitude, yielding a magnetic polarity sequence (Fig. 11). This polarity sequence was correlated to the geological time scale 2004 (GTS 2004) by Gradstein et al. (2004). The magnetozones of the Oytag section well correlate with the polarity chrons from C7n.2n to C29r, covering an age interval of 65.5–24.2 Ma (Fig. 11).

Based on the magnetostratigraphic time scale, the sedimentation rates of the section can be calculated (Fig. 12). Because the studied succession is mostly made up by continental deposits of gravels, sandstone, siltstones, mudstone and gypsum, and the studied region is in an active tectonic region, therefore, the sedimentation rates should be highly variable. Fig. 12 indicates that the sedimentation rates vary from 74 to 172 m/Ma. The highest rate corresponds to the lower molasse deposits (generally from 3020 to 2620 m), due to the high energy transportation and quick accumulation. However, the upper molasse deposits (above 740 m) do not correspond to a high sedimentation rate, and this is due to the sedimentary hiatus at the bottom of the molasse deposits (Figs. 3 and 12).

Moreover, the long-term seawater Sr/Ca curve has been well constructed, which indicated that seawater Sr/Ca was higher (about 1.5 times the modern value) in the late Cretaceous (75–65 Ma) than at any time in the Cenozoic (Lear et al., 2003). Fig. 13 indicates that the seawater Sr/Ca ratio falls between 14 and 9.5 during the late Cretaceous, whereas it is less than 9.5 during the Cenozoic. In this study, eighteen samples were collected for Ca and Sr analyses from the in situ (not the detrital limestone boulders) limestone Beds III, IV, and V. The measured Sr/Ca ratio of the limestone Bed III has a mean value of 8.95 (n = 10), falling into the range of Cenozoic seawater Sr/Ca ratio, being less than that of the late Cretaceous (Fig. 13), and this further demonstrates that the boulder with late Cretaceous rudist fossils within the limestone Bed III is of detrital origin. Additionally, the mean Sr/Ca values from the in situ limestone Beds IV and V are 8.5 (n = 4) and 8.2 (n = 4), respectively. Based on the magnetostratigraphic time scale, these values well match the early Eocene seawater Sr/Ca ratios (Fig. 13). The above lines of evidence further suggest that the new geomagnetic polarity time scale of the Oytag section is reliable.


**Fig. 10.** Photo shows the detrital boulder containing a marine fossil of rudist (bottom left corner); such fossils are not in situ.

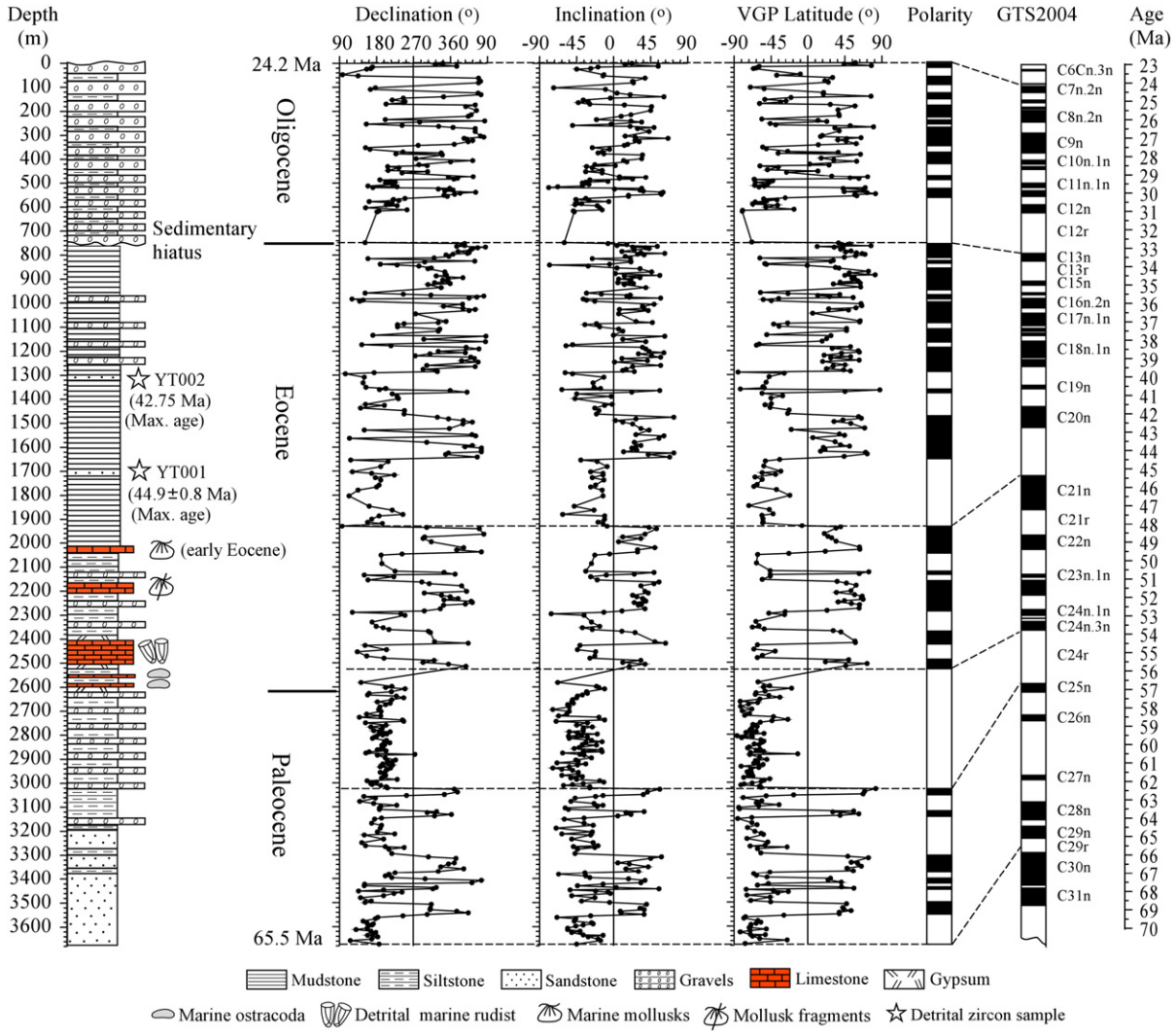


**Fig. 11.** Magnetostratigraphy of the Oytag section. Magnetic polarity is compared with the geological time scale of GTS2004 (Gradstein et al., 2004). The marine mollusk fauna at a depth of 2030 m suggests an early Eocene age.

## 5. Discussions

### 5.1. Paleogene tectonics in the Pamir Plateau and the Tarim Basin

The Pamir Plateau is located in the western end of the India–Eurasia collision zone (Fig. 14a) as a result of convergence between the Pamir Plateau and Tian Shan (Molnar and Tapponnier, 1975). The Cenozoic crustal shortening in the Pamir Plateau can be up to 300–400 km (Burtman, 2000; Burtman and Molnar, 1993), being about one fifth of the 2000 to 2500 km crustal shortening between the India and Eurasia plates (Besse and Courtillot, 1988; Besse et al., 1984; Harrison et al., 1992; Le Pichon et al., 1992; Patrait and Achache, 1984). At present, the Pamir Plateau separates the Tadjik and the Tarim Basins (Fig. 14a), however, Burtman and Molnar (1993) argued that the northern margin of the Pamir Plateau had advanced over the Tadjik Basin for more than 300 km since the Paleogene time. Therefore, before the northward displacement of the Pamir Plateau relative to Tian Shan, these two basins were connected.

Early Eocene marine limestone can be found in the Tarim Basin (Fig. 14b). The early Eocene Tarim Sea was connected with the Tadjik Sea, belonging to the enormous Turan Sea and connecting with the other parts of the Neotethys Ocean. In the Tarim Basin, the sea water came from the west. Considering the 300–400 km crustal shortening between the Pamir Plateau and the Tian Shan ranges, there would exist a wide gateway and enabled sea water exchanges. This can be supported by the very similar marine bivalve fossils among France, Turkey and the Tarim Basin. In this sense, the interbedded marine deposits in the Oytag section offer opportunity for studying marine transgression history in the Tarim Basin.

### 5.2. Stepwise sea retreat from the southwest Tarim Basin in the early Eocene

The Pamir Plateau is marked by intense tectonics and crustal shortening. Additionally, remarkable global climate changes also occur in the Cenozoic era. One of the most important geological issues in central Asia is the timing of the gradual retreat of an epicontinental sea that once extended from Europe to Asia (Bosboom et al., 2011; Piller et al., 2007; Popov et al., 2006; Ritts et al., 2008; Rögl, 1999; Schulz et al., 2005; Vasiliev et al., 2004). It is important to study the timing and causes of the seawater retreat out of the southwest Tarim Basin before the northward displacement of the Pamir Plateau. Our record indicates that there are five marine limestone layers interbedded in the Oytag section (Fig. 15), indicating five transgression–regression cycles in the region studied. According to our magnetostratigraphic time scale, nearly all the five marine transgressions occurred in the early Eocene. Further linear interpolation between the magnetic chrons of C21n and C24n.3n yields absolute age and duration for each cycle (Fig. 15). The

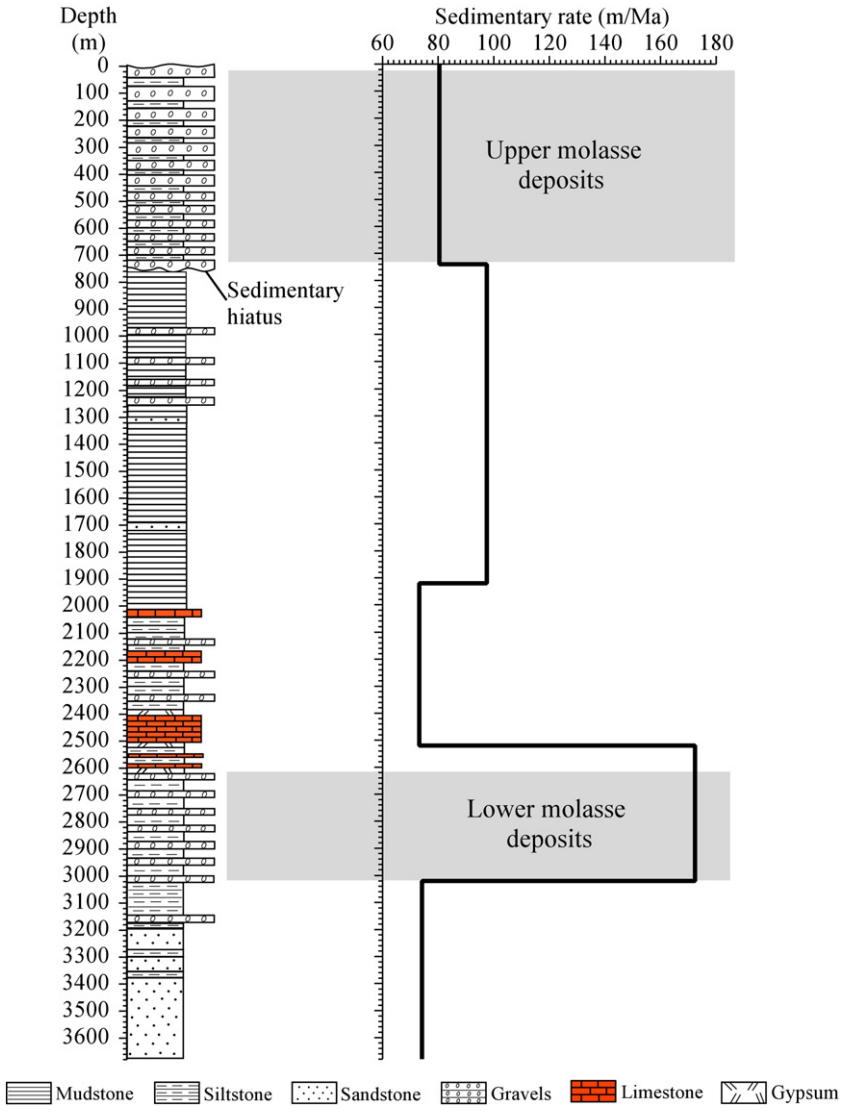


**Fig. 12.** Variations of sedimentation rate of the Oytag section. Note the sedimentary hiatus at the base of the upper molasse deposits.

first transgression–regression cycle occurred at 54.8 Ma (Phase I), and the second sea transgression occurred at ca. 54.6 Ma (Phase II). Different from the two previous short-term sea transgression phases, the third phase had the longest time of sea transgression and started from 53.8 to 52.1 Ma, thus lasting 1.7 Ma. The fourth sea transgression occurred at 49–48.6 Ma, lasting 0.4 Ma. The finial sea transgression occurred at 46.9–46.6 Ma, lasting 0.3 Ma (Fig. 15). Therefore, although the timing of the sea retreat from the Tarim Basin may be diachronous, the final sea retreat from the studied region occurred at ca. 46.6 Ma.

It is important to discuss the causes of the stepwise sea retreat out of the studied region. During the Cenozoic era, dramatic climatic events can lead to large scale global eustatic sea level fluctuations of more than 200 m during the Cenozoic even without tectonism (Miller et al., 2005). The five cycles of transgression and regression were correlated to the global eustatic sea level fluctuations (Fig. 15). Previous studies have suggested that the early Eocene was marked by a climatic optimum (Miller et al., 1987; Zachos et al., 2001) and the maximum Cenozoic marine transgression (Haq et al., 1987; Kominz et al., 2008; Miller et al., 2005; Van Sickel et al., 2004). The five sea transgression phases at Oytag correlate well with the global scale eustatic sea level fluctuations in the early Eocene, and the longest-time of the Cenozoic sea transgression in the Tarim basin corresponds to the highest sea level which occurred at about 53.8–52 Ma (Fig. 15). Such evidence demonstrates that the stepwise sea retreat from the studied region was mainly a response to global eustatic sea-level fluctuations before the northward displacement of the Pamir Plateau. Additionally, the Oytag section is located in an active tectonic region, and in this context, tectonically induced basin depression may play a minor role in controlling sea transgressions.

### 5.3. Uplift history in the northern margin of the Tibetan Plateau

The southwestern Tarim Basin currently receives sediments from the northern margin of the Tibetan Plateau (Fig. 1b), and it is natural to use the basin's Cenozoic strata as a proxy to decipher the uplift history of the northern Tibet (Yin et al., 2002). In this sense, the Cenozoic deposits at Oytag not only document marine transgressions and regressions but also document tectonic uplift and crustal shortening in the Pamir Plateau. The earliest molasse deposits of up to 420 m thick broadly correspond to the magnetic chron C24r (Fig. 11), having an age range of 56.7–53.8 Ma, but is centered at ca. 55 Ma. Such coarse conglomerates are derived from the Pamir Plateau and transported by high-energy flows in high-gradient depositional systems, suggesting the early uplift of the northwestern margin of Tibetan Plateau being at ca. 55 Ma. It is consistent with the initial hard collision between the India and Eurasia plates (e.g., Klootwijk et al., 1992). However, because sea

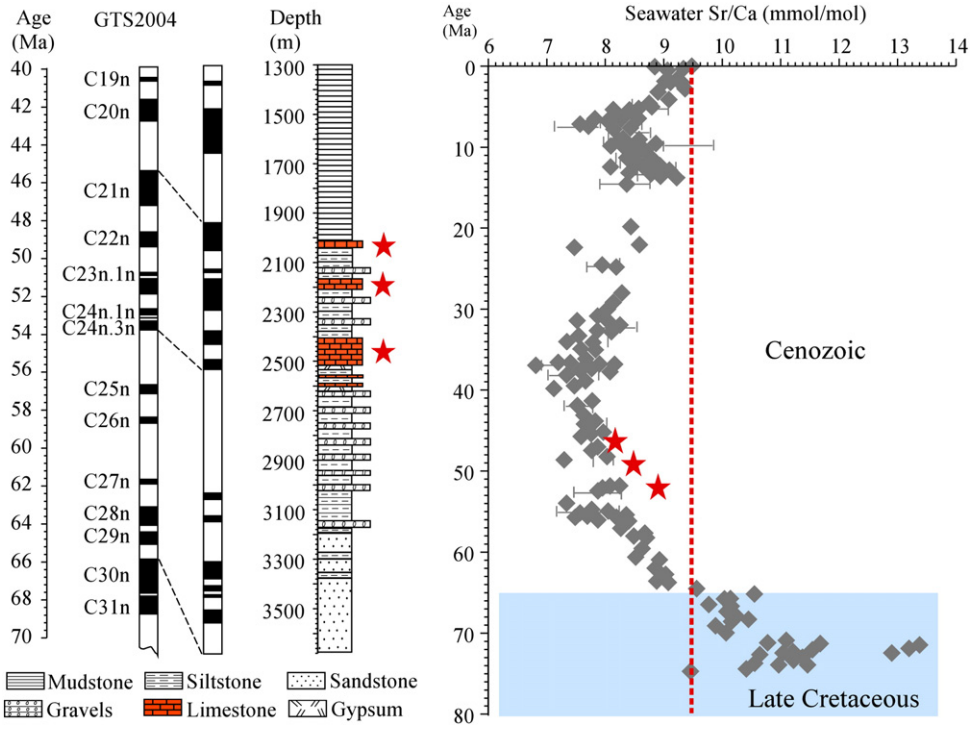


**Fig. 13.** Seawater Sr/Ca record from the late Cretaceous to the Cenozoic. The red stars indicate the mean Sr/Ca ratios from the limestone Beds III to V. Data are from Lear et al. (2003).

transgressions in the southwest Tarim Basin occurred between 54.8 and 46.6 Ma, this early uplift preceded the termination of marine carbonate deposition, and there still existed a wide gateway between the Pamir Plateau and the Tian Shan after this early tectonic uplift.

Moreover, although the latest marine regression at Oytag occurred at ca. 47 Ma, the deposits from 47 Ma to the boundary of Eocene/Oligocene (34 Ma) is dominated by lacustrine mudstone, and the fine particle size of the sediments indicates that they were transported by low-energy flows from low-gradient depositional systems. Therefore, since the final retreat of the sea water from the southwest Tarim Basin to the end of the Eocene, there was no prominent crustal shortening between the Pamir Plateau and Tian Shan, and this relatively stable tectonic episode lasted to the end of the Eocene.

From 34 Ma to the late Oligocene, coarse molasse deposits accumulated in the southwestern margin of the Tarim Basin, with a thickness of more than 750 m (Fig. 11). The coarse conglomerates in this foreland basin were pluvial fan accumulation representing proximal sources and increased relief gradient. These molasse deposits indicate accelerated tectonic uplift in the Pamir Plateau as well as accelerating convergence between the Pamir Plateau and Tian Shan.

This can be further demonstrated by other lines of evidence. Firstly, the pollen percentage of *Picea* at Oytag shows remarkable increase after 34 Ma ago, whereas its percentage is generally lower than 20% earlier than that time (Fig. 16a). Previous studies suggested that the abundance of *Picea* of greater than 20% indicates the occurrence of a sub-alpine coniferous forest (Dupont-Nivet et al., 2008; Weng et al., 1993). Based on the spatial pattern of the *Picea* surface pollen distribution along the elevation gradient in Tibet and Xinjiang (Fig. 16b), Lu et al. (2008) indicates that high *Picea* percentages (>30%) occur

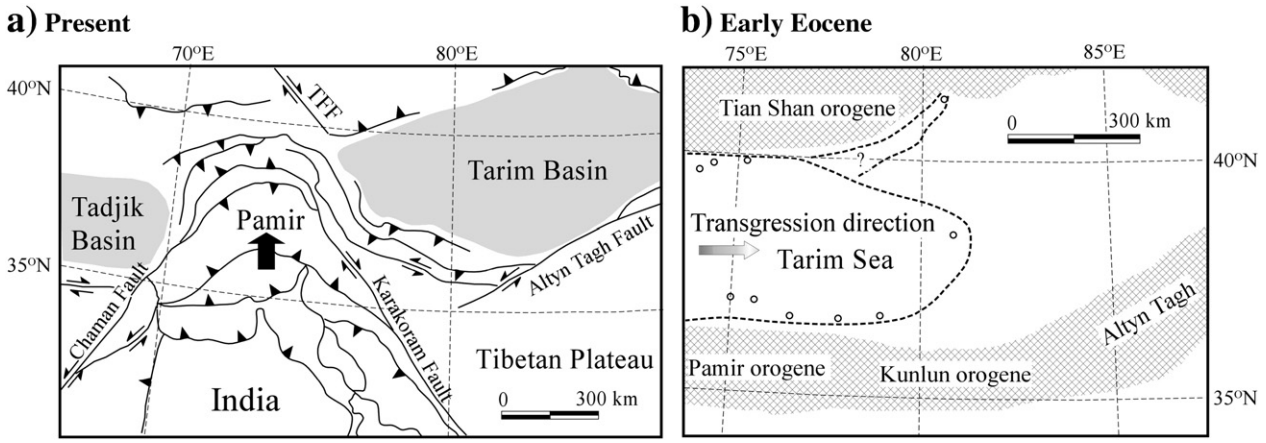


**Fig. 14.** Maps showing tectonics in the Pamir Plateau and the early Eocene marine transgression in the Tarim Basin. (a) The present tectonic framework in the vicinity of the Pamir Plateau; note the northward thrusting of the Pamir Plateau separating the Tadjik and the Tarim Basins. (b) The reconstructed Tarim Sea in the early Eocene; the open circle indicates sites with early Eocene marine limestone.

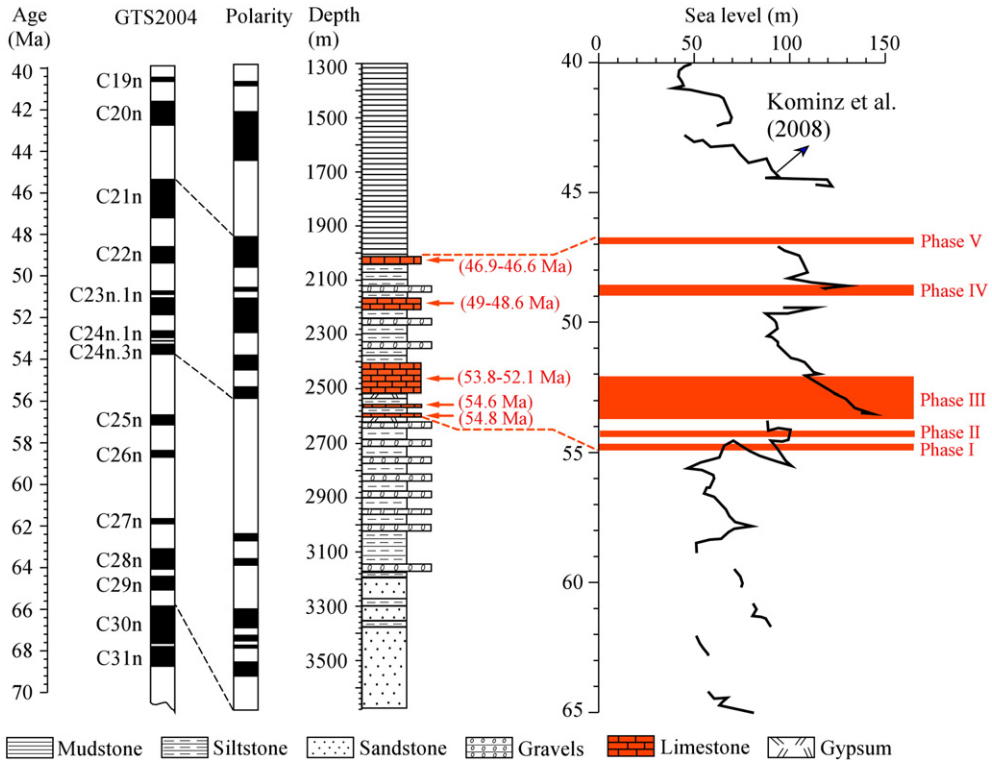


**Fig. 15.** The five cycles of marine transgressions and regressions recorded in the Oytag section (brown shadow) and their correlation with the global eustatic sea-level fluctuations. Eustatic sea level data are from Kominz et al. (2008).

between 3000 and 4000 m above sea level (Fig. 16c). Therefore the high percentage of *Picea* within the analyzed sequence suggests that the elevation of the Pamir Plateau might reach 3000 m above sea level at 34 Ma. Moreover, previous studies have suggested that a high percentage of *Picea* (20 to 50%) decreased abruptly outside the sub-alpine forest (Sugita, 1993), suggesting that the *Picea* pollen is not far traveled but from the nearby mountains. This implies that the northern edge of the Pamir Plateau not only uplifted rapidly since 34 Ma but also moved close to the studied site, further supporting our view that the convergence between the Pamir Plateau and Tian Shan ranges accelerated since 34 Ma ago.

Additionally, Burtman and Molnar (1993) argued that the northward displacement of the North Pamir Plateau started in the late Eocene. Detrital apatite fission-track data from the foreland basin of the western Kunlun range indicate that cooling in the source terrain was under way by the early Oligocene (Sobel and Dumitru, 1997). Yin et al. (2002) studied the Cenozoic deposits of the similar foreland basin which indicates that rapid basin subsidence relative to mountain uplift started at ca. 37 Ma. Cowgill (2010) suggested that the Kashgar–Yecheng right-slip faulting system along the eastern margin of the Pamir Plateau was active by ca. 37 Ma. Given the fact that the uncertainties between different dating methods do exist, the above studies demonstrate that the latest Eocene to the early Oligocene was marked by intensive tectonic crustal shortening in the northern Pamir Plateau.

## 6. Conclusions

The Pamir Plateau lies in the western end of the India–Eurasia collision zone, characterized by significant crustal shortening, mountain building, and paleoenvironmental changes. In this study, we used multiple dating methods to constrain the timing of seawater retreat from the southwest Tarim Basin as well as the uplift history in the northern edge of the Pamir Plateau. The following conclusions can be drawn from the present investigation of the Oytag section in the foreland basin of the Pamir–Kunlun range.

(1) Based on biostratigraphic age control, U–Pb ages of detrital zircons, and magnetostratigraphy, we yielded high resolution chronology for the early Cenozoic marine–terrestrial sediments at Oytag, providing the basis for discussing tectonics and the seawater retreat from the southwest Tarim Basin.
(2) Five marine transgression and regression cycles at 54.8 Ma, 54.6 Ma, 53.8–52.1 Ma, 49–48.6 Ma, and 46.9–46.6 Ma were identified in the region studied, mostly in response to global eustatic sea level fluctuations during the early Eocene. Although the Cenozoic sea retreat from the Tarim Basin may be diachronous, the final sea water retreat from the studied site occurred at about 47 Ma.
(3) Sedimentary evidence indicates that the early uplift of the northern edge of the Tibetan Plateau occurred at about 55 Ma, but this uplift preceded the retreat of the Neotethys Ocean in the Pamir Plateau. Another uplift episode started 34 Ma, evidenced by the accumulation of coarse molasse deposits in the foreland basin and our pollen record, suggesting the accelerated convergence between the Pamir Plateau and the Tian Shan ranges since the beginning of the early Oligocene.

## Acknowledgments

We thank J.L. Li for the helpful discussions and L.Q. Xie and Z.Y. Zhang for the field assistance. This work was supported by the "Strategic Priority Research Program" of the Chinese Academy of Sciences, grant no. XDB03020500, the National Basic Research Program of China (2010CB833400), and the National Nature Science Foundation of China (grants 40830104 and 41272203). We are grateful to the anonymous reviewers for their detailed and thoughtful reviews that improved the manuscript greatly.

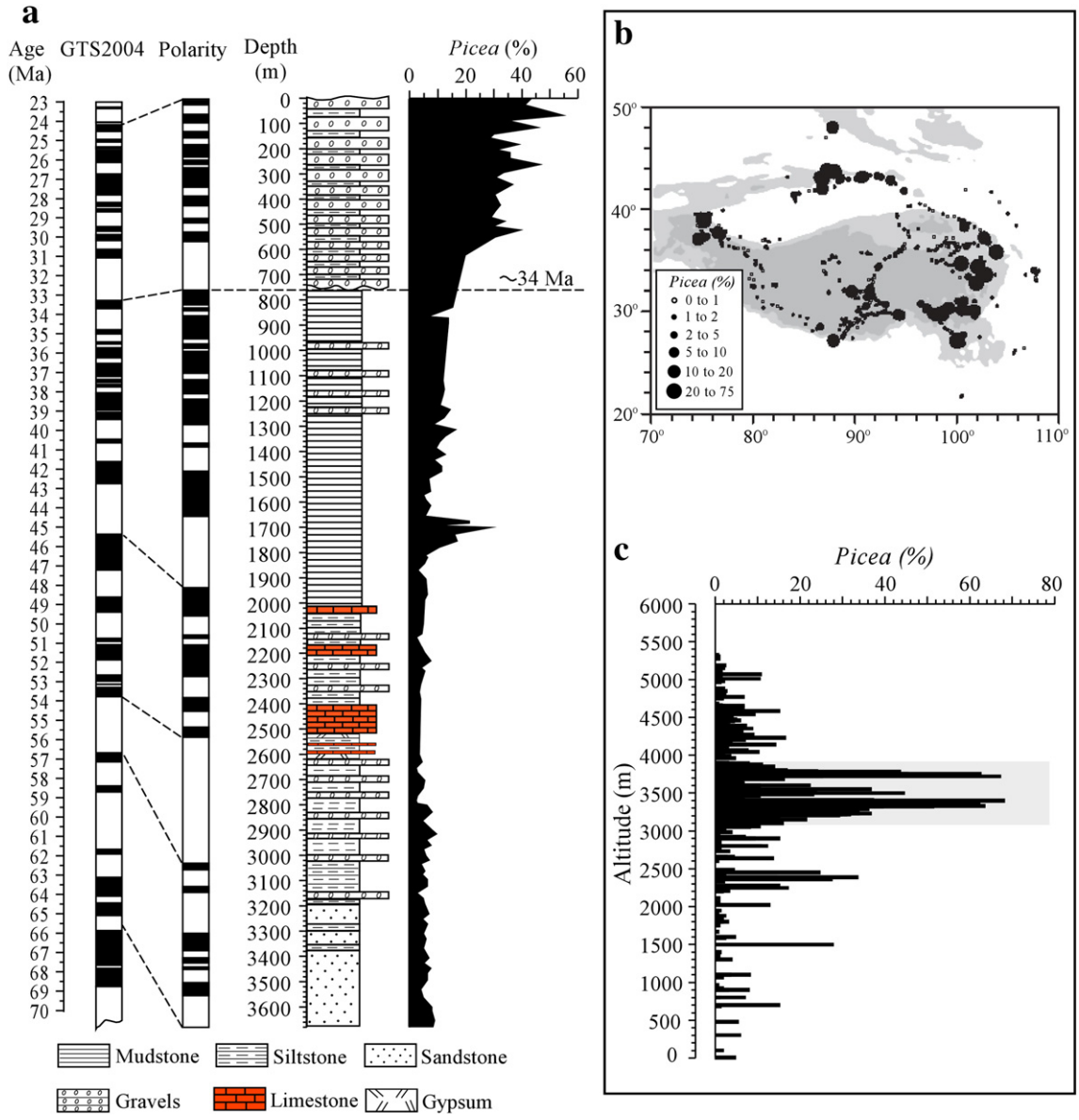


**Fig. 16.** Vertical variations of *Picea* pollen of the Oytag section and its implications. a: Percentages of *Picea* pollen showing remarkable increase after 34 Ma. b: Modern *Picea* distributions in Tibet and the Tian Shan range (Lu et al., 2008). c: Pollen abundances (%) of *Picea* versus elevation in the Tibetan Plateau (Lu et al., 2008).

## References


Abers, G., Bryan, C., Roecker, S., McCaffrey, R., 1988. Thrusting of the Hindu Kush over the Southeastern Tadjik Basin, Afghanistan: evidence from two large earthquakes. Tectonics 7, 41–56.

Bershaw, J., Garzione, C.N., Schoenbohm, L., Gehrels, G., Tao, L., 2012. Cenozoic evolution of the Pamir plateau based on stratigraphy, zircon provenance, and stable isotopes of foreland basin sediments at Oytag (Wuyitake) in the Tarim Basin (west China). Journal of Asian Earth Sciences 44, 136–148.

Besse, J., Courtillot, V., 1988. Paleogeographic maps of the continents bordering the Indian Ocean since the Early Jurassic. Journal of Geophysical Research 93, 11791–11808.

Besse, J., Courtillot, V., Pozzi, J.P., Westphal, M., Zhou, Y.X., 1984. Palaeomagnetic estimates of crustal shortening in the Himalayan thrusts and Zangbo suture. Nature 311, 621–626.

Bosboom, R.E., Dupont-Nivet, G., Houben, A.J.P., Brinkhuis, H., Villa, G., Mandic, O., Stoica, M., Zachariasse, W.J., Guo, Z., Li, C., Krijgsman, W., 2011. Late Eocene sea retreat from the Tarim Basin (west China) and concomitant Asian paleoenvironmental change. Palaeogeography, Palaeoclimatology, Palaeoecology 299, 385–398.

Burtman, V.S., 2000. Cenozoic crustal shortening between the Pamir and Tien Shan and a reconstruction of the Pamir–Tien Shan transition zone for the Cretaceous and Palaeogene. Tectonophysics 319, 69–92.

Burtman, V.S., Molnar, P., 1993. Geological and geophysical evidence for deep subduction of continental crust beneath the Pamir. Geological Society of America Special Papers 281, 1–76.

Burtman, V.S., Skobelev, S.F., Molnar, P., 1996. Late Cenozoic slip on the Talas–Ferghana fault, the Tien Shan, Central Asia. Geological Society of America Bulletin 108, 1004–1021.

Collinson, D.W., 1983. Methods in Rock Magnetism and Palaeomagnetism: Techniques and Instruments. Chapman & Hall, London.

Cowgill, E., 2010. Cenozoic right-slip faulting along the eastern margin of the Pamir salient, northwestern China. Geological Society of America Bulletin 122, 145–161.

Dupont-Nivet, G., Hoorn, C., Konert, M., 2008. Tibetan uplift prior to the Eocene–Oligocene climate transition: evidence from pollen analysis of the Xining Basin. Geology 36, 987–990.

Faegri, K., Iversen, J., 1989. Textbook of Pollen Analysis. John Wiley & Sons, New York.

Fisher, R.A., 1953. Dispersion on a sphere. Proceedings. Royal Society of London Series A 217, 295–305.

Fu, B.H., Ninomiya, Y., Guo, J.M., 2010. Slip partitioning in the northeast Pamir–Tian Shan convergence zone. Tectonophysics 483, 344–364.

Gradstein, F., Ogg, J., Smith, A., 2004. A Geologic Time Scale 2004. Cambridge University Press, Cambridge.

Hanchar, J.M., Miller, C.F., 1993. Zircon zonation patterns as revealed by cathodoluminescence and backscatterd electron images: implications for interpretation of complex crustal histories. Chemical Geology 110, 1–13.

Haq, B.U., Hardenbol, J., Vail, P.R., 1987. Chronology of fluctuating sea levels since the Triassic (250 million years ago to present). Science 235, 1156–1167.

Harrison, T.M., Copeland, P., Kidd, W.S.F., Yin, A., 1992. Raising Tibet. Science 255, 1663–1670.

Kirschvink, J., 1980. The least square line and the analysis of paleomagnetic data. Geophysical Journal of the Royal Astronomical Society 62, 699–718.
Klootwijk, C.T., Gee, J.S., Peirce, J.W., Smith, G.M., McFadden, P.L., 1992. An early India–Asia contact: paleomagnetic constraints from Ninetyeast Ridge, ODP Leg 121. Geology 20, 395–398.
Kominz, M.A., Browning, J.V., Miller, K.G., Sugarman, P.J., Mizintseva, S., Scotese, C.R., 2008. Late Cretaceous to Miocene sea-level estimates from the New Jersey and Delaware coastal plain coreholes: an error analysis. Basin Research 20, 211–226.
Lan, X., Wei, J.M., 1995. Late Cretaceous–Early Tertiary Marine Bivalve Fauna from the Western Tarim Basin. Science Press, Beijing.
Le Pichon, X., Fournier, M., Jolivet, L., 1992. Kinematics, topography, shortening, and extrusion in the India–Eurasia collision. Tectonics 11, 1085–1098.
Lear, C.H., Elderfield, H., Wilson, P.A., 2003. A Cenozoic seawater Sr/Ca record from benthic foraminiferal calcite and its application in determining global weathering fluxes. Earth and Planetary Science Letters 208, 69–84.
Lu, H.Y., Wu, N.Q., Yang, X.D., Shen, C.M., Zhu, L.P., Wang, L., Li, Q., Xu, D.K., Tong, G.B., Sun, X.J., 2008. Spatial pattern of Abies and Picea surface pollen distribution along the elevation gradient in the Qinghai–Tibetan Plateau and Xinjiang, China. Boreas 37, 254–262.
Miller, K.G., Fairbanks, R.G., Mountain, G.S., 1987. Tertiary oxygen isotope synthesis, sea level history, and continental margin erosion. Paleoceanography 2, 1–19.
Miller, K.G., Kominz, M.A., Browning, J.V., Wright, J.D., Mountain, G.S., Katz, M.E., Sugarman, P.J., Cramer, B.S., Christie-Blick, N., Pekar, S.F., 2005. The Phanerozoic record of global sea-level change. Science 310, 1293–1298.
Molnar, P., Tapponnier, P., 1975. Cenozoic tectonics of Asia: effects of a continental collision. Science 189, 419–426.
Negredo, A.M., Replumaz, A., Villasenor, A., Guillot, S., 2007. Modeling the evolution of continental subduction process in the Pamir–Hindu Kush region. Earth and Planetary Science Letters 259, 212–225.
Okan, Y., Hosgor, I., 2009. Early Eocene (Middle–Late Cuisian) molluscs assemblage from the harpactocarcinid beds, in the Yoncali Formation of the Cankiri Basin, Central Anatolia, and implications for tethys paleogeography. Geological Bulletin of Turkey 52, 1–30.
Pan, Y.S., 2000. Geological Evolution in the Karakorum and Kunlun Mountains. Science Press, Beijing.
Patrait, P., Achache, J., 1984. India—Eurasia collision chronology has implications for crustal shortening and driving mechanism of plates. Nature 311, 615–621.
Piller, W.E., Harzhauser, M., Mandic, O., 2007. Miocene central Paratethys stratigraphy — current status and future directions. Stratigraphy 4, 151–168.
Popov, S.V., Shcherba, I.G., Ilyina, L.B., Nevesskaya, L.A., Paramonova, N.P., Khondkarian, S.O., Magyar, I., 2006. Late Miocene to Pliocene palaeogeography of the Paratethys and its relation to the Mediterranean. Palaeogeography, Palaeoclimatology, Palaeoecology 238, 91–106.
Ritts, B., Yue, Y., Graham, S., Sobel, E., Abbink, O.A., Stockli, D., 2008. From sea level to high elevation in 15 million years. American Journal of Science 308, 657–678.
Robinson, A.C., Yin, A., Manning, C.E., Harrison, T.M., Zhang, S.H., Wang, X.F., 2004. Tectonic evolution of the northeastern Pamir: constraints from the northern portion of the Cenozoic Kongur Shan extensional system, western China. Geological Society of America Bulletin 116, 953–973.
Robinson, A.C., Yin, A., Manning, C.E., Harrison, T.M., Zhang, S.H., Wang, X.F., 2007. Cenozoic evolution of the eastern Pamir: implications for strain-accommodation mechanisms at the western end of the Himalayan–Tibetan orogen. Geological Society of America Bulletin 119, 882–896.
Rögl, F., 1999. Mediterranean and Paratethys facts and hypotheses of an Oligocene to Miocene paleogeography (short overview). Geologica Carpathica 50, 339–349.
Schulz, H.M., Bechtel, A., Sachsenhofer, R.F., 2005. The birth of the Paratethys during the Early Oligocene: from Tethys to an ancient Black Sea analogue? Global Planet. Change 49, 163–176.
Scott, R.W., Wan, X.Q., Sha, J.G., Wen, S.X., 2010. Rudists of Tibet and the Tarim basin, China: significance to Requieniidae phylogeny. Journal of Paleontology 84, 444–465.
Sobel, E.R., Dumitru, T.A., 1997. Thrusting and exhumation around the margins of the western Tarim basin during the India–Asia collision. Journal of Geophysical Research 102 (B3), 5043–5063.
Sugita, S., 1993. A modern pollen source area from an entire lake surface. Quaternary Research 39, 239–244.
Sun, J.M., Liu, T.S., 2006. The age of the Taklimakan Desert. Science 312, 1621.
Sun, J.M., Zhang, L.Y., Deng, C.L., Zhu, R.X., 2008. Evidence for enhanced aridity in the Tarim Basin of China since 5.3 Ma. Quaternary Science Reviews 27, 1012–1023.
Sun, J.M., Zhang, Z.Q., Zhang, L.Y., 2009. New evidence on the age of the Taklimakan Desert. Geology 37, 159–162.
Tang, T.F., Xue, Y.S., Yü, C.L., 1992. Characteristics and Sedimentary Environments of the Late Cretaceous to Early Tertiary Marine Strata in the Western Tarim Basin. Science Press, Beijing, China.
Tapponnier, P., Xu, Z.Q., Roger, F., Meyer, B., Arnaud, N., Wittlinger, G., Yang, J.S., 2001. Oblique stepwise rise and growth of the Tibet Plateau. Science 294, 1671–1677.
Van Sickel, W.A., Kominz, M.A., Miller, K.G., Browning, J.V., 2004. Late Cretaceous and Cenozoic sea-level estimates: backstripping analysis of borehole data, onshore New Jersey. Basin Research 16, 451–465.
Vasiliev, I., Krijgsman, W., Langereis, C.G., Panaiotu, C.E., Matenco, L., Bertotti, G., 2004. Towards an astrochronological framework for the eastern Paratethys Mio–Pliocene sedimentary sequences of the FocYani basin (Romania). Earth and Planetary Science Letters 227, 231–247.
Weng, C.Y., Sun, X.J., Chen, Y.S., 1993. Numerical characteristic of pollen assemblages of surface samples from the west Kunlun Mountains. Acta Botânica Sinica 35, 69–79.
Xie, L.W., Zhang, Y.B., Zhang, H.H., Sun, J.F., Wu, F.Y., 2008. In situ simultaneous determination of trace elements, U–Pb and Lu–Hf isotopes in zircon and baddeleyite. Chinese Science Bulletin 53, 1565–1573.
Yin, A., Harrison, T.M., 2000. Geologic evolution of the Himalayan–Tibetan orogen. Annual Review of Earth and Planetary Sciences 28, 211–280.
Yin, A., Rumelhart, P.E., Butler, R., Cowgill, E., Harrison, T.M., Foster, D.A., Ingersoll, R.V., Zhang, Q., Zhou, X., Wang, X., Hanson, A., Raza, A., 2002. Tectonic history of the Altyn Tagh fault system in northern Tibet inferred from Cenozoic sedimentation. Geological Society of America Bulletin 114, 1257–1295.
Zachos, J.C., Pagani, M., Sloan, L., Thomas, E., Billups, K., 2001. Trends, rhythms, and aberrations in global climate 65 Ma to present. Science 292, 686–693.
Zheng, H.B., Tada, R., Jia, J.T., Lawrence, C., Wang, K., 2010. Cenozoic sediments in the southern Tarim Basin: implications for the uplift of northern Tibet and evolution of the Taklimakan Desert. Special Publication. Geological Society of London 342, 67–78.